Science Advances
AAAS

advances.sciencemag.org/cgi/content/full/6/46/eabc2414/DC1

# Supplementary Materials for

## Combined high- and low-latitude forcing of East Asian monsoon precipitation variability in the Pliocene warm period

Yichao Wang, Huayu Lu*, Kexin Wang, Yao Wang, Yongxiang Li, Steven Clemens, Hengzhi Lv, Zihan Huang, Hanlin Wang, Xuzhi Hu, Fuzhi Lu, Hanzhi Zhang

*Corresponding author. Email: huayulu@nju.edu.cn

Published 13 November 2020, *Sci. Adv.* **6**, eabc2414 (2020)
DOI: 10.1126/sciadv.abc2414

**The PDF file includes:**

Supplementary Materials Part 1 and Part 2
Figs. S1 to S8
Table S1
Legend for data S1
References

**Other Supplementary Material for this manuscript includes the following:**

(available at advances.sciencemag.org/cgi/content/full/6/46/eabc2414/DC1)

Data S1

# Supplementary Materials

## Part 1. Sedimentology and depositional environment of the CGC site

From the bottom to the top, samples were collected from three subsections at the CGC site, within the same gully.

### 1.1 Site CGC-3 34.3147°N, 109.5087°E

Site CGC-3 (Fig. S1, right) is the lowest part of the CGC sequence. The total thickness is 137.5 m, with a dip direction of 165 ° and an inclination of 13 °. The entire profile is characterized by the frequent alternation of fine-grained massive sandy mudstone (Fm) and coarse sediments (sandstone (Sm), conglomeratic massive sandstone (Sm+c), massive or crudely-bedded sandy clast-supported conglomerate (Gm)). Pale olive (5Y6/3) mottles are common in the fine-grained massive sandy mudstone (Fm). The sequence indicates a typical sedimentary environment with frequent alternations of flood flows and overbank deposition. The upper 10 m is reddish brown (5YR4/4) mudstone (Md), similar to site CGC-2 and the bottom part of site CGC-1.

### 1.2 Site CGC-2 34.3101°N, 109.5057°E

Site CGC-2 (Fig. S1, middle) is the middle part of the CGC depositional sequence, located ~580 m southwest of site CGC-3. The total thickness is 40 m, with a dip direction of 160° and an inclination of 8°. The lithology is mainly reddish-brown (5YR4/4) mudstone (Md) with overlying dark reddish brown (2.5YR3/3) clay sediments (Cly) which are much finer and darker than the massive sandy mudstone (Fm); the weakly-laminated silt and clay may indicate a water-lain settling. The thick reddish brown mudstone and dark reddish brown clay may result from suspension settling in shallow lake environments that were usually below wave base, or in areas with weak wave energy, but not deep enough to

provide reducing conditions; they were later modified by post-depositional reddening under oxidizing conditions.

There are three sets of gravel (Gm) or conglomeratic sandstone (Sm+c) layers at the bottom, middle and top, respectively. The conglomerate facies are mainly massive or crudely-bedded sandy clast-supported conglomerate (Gm). This facies was produced by gravel-bed streams or low-relief longitudinal bars. The clasts are sub-rounded to rounded, with a better roundness and sorting ranging from 5-10 cm. The pale olive mottling associated with root activity is less frequent in the mudstone (Md) and in the massive sandy mudstone (Fm), indicating reduced subaerial exposure in a less energetic sedimentary environment. There is a mudstone layer beneath the lowest sandy conglomerate layer; however, deeper sampling was not possible and therefore we collected samples from site CGC-3, which is below CGC-2, from field observation. The upper part of CGC-2 consists of two conglomeratic sand and gravel layers interbedded with a mudstone layer, which is similar to the lower part of CGC-1. The lower part is 15-cm-thick dark reddish-brown (2.5YR3/3) clay sediments (Cly) and underlying thick reddish-brown (5YR4/4) mudstone (Md).

### 1.3 Site CGC-1 34.3053°N, 109.5006°E

Site CGC-1 (Fig. S1, left) is the upper part of the CGC sequence, located ~710 m southwest of site CGC-2, with a dip direction of 160° and an inclination of 8°. The total thickness is 109.5 m. The major lithology is thick yellowish red (5YR6/6) sandy mudstone with interbedded yellow (10YR8/6) conglomeratic sand layers, or occasional gravel layers. Fine-grained deposits are generally pervasive, sheet-like and extend laterally for tens of meters; they are composed of massive sandy mudstone (Fm). Gradational contacts indicated by color and lithology are common within the fine-grained units, but the

boundaries between fine-grained units (Fm, Fm+c) and coarse units (Gm, Gms, Sm+c) are always sharp. Paleosol is present, with a massive structure and pale olive (5Y6/3) mottling, which is common in the fine-grained units, and typically occurs as anastomosing networks or patches. In some cases, the mudstone and sandy mudstone can be conglomeratic or gritty (Fm+c), which is also structureless, due to post-depositional processes such as pedogenesis and bioturbation, caused by large tetrapods walking on a floodplain (*14*). We recognize this fine-grained facies association as floodplain deposits, in the form of suspension settling during lower flow regimes and waning floods (*47*). In addition, the 10-m-thick reddish brown (5YR4/4) mudstone (Md) with overlying 20-cm-thick dark reddish brown (2.5YR3/3) clay sediments (Cly) at the bottom of the CGC-1 section is much finer than the massive sandy mudstone (Fm). Lithologies are mixtures of clay and silt, without sand clasts. It is used as a marker layer to correlate with the top part (CGC-2) of the whole sequence. The top 20 cm of dark reddish-brown (2.5YR3/3) clay sediments (Cly) show weak laminations, indicating original structures. This thick mudstone indicates a consistently wet environment with minor fluctuations (*47*), and is defined as a shallow lake deposit.

Coarse-grained deposits are composed of crudely horizontally-stratified clast-supported conglomerates (Gm), matrix-supported conglomerate (Gms), conglomeratic sandstone (Sm+c), and massive sandstone (Sm). The conglomerate facies are mainly massive or crudely-bedded sandy clast-supported conglomerate (Gm). The clasts are sub-rounded to rounded. The conglomerate beds can vary from 1 m to 4 m in thickness and can extend laterally for tens of meters. The conglomerate facies are usually accompanied by conglomeratic sandstone (Sm+c) and massive sandstone (Sm). The basal boundaries of the units are usually sharp. The wide distribution of particle size, erosional bases, and weak stratification indicate gravel-bed streams or low-relief longitudinal bars with highly concentrated sediment dispersion and high-magnitude flood events (*48*). At some levels,

the conglomerate facies occur in the form of matrix-supported conglomerate (Gms), which reflects poor sorting, a clay to pebble matrix, with almost no imbrication and lacking cross-stratification; it has a sharp contact with the upper and lower strata. The thickness of this facies is up to 4 m. Gms appear to be ungraded and have variable clast sizes, with the range of 5-40 cm, with floating outsized clasts in the mud matrix, indicating that it was deposited by debris flows on alluvial fan lobes.

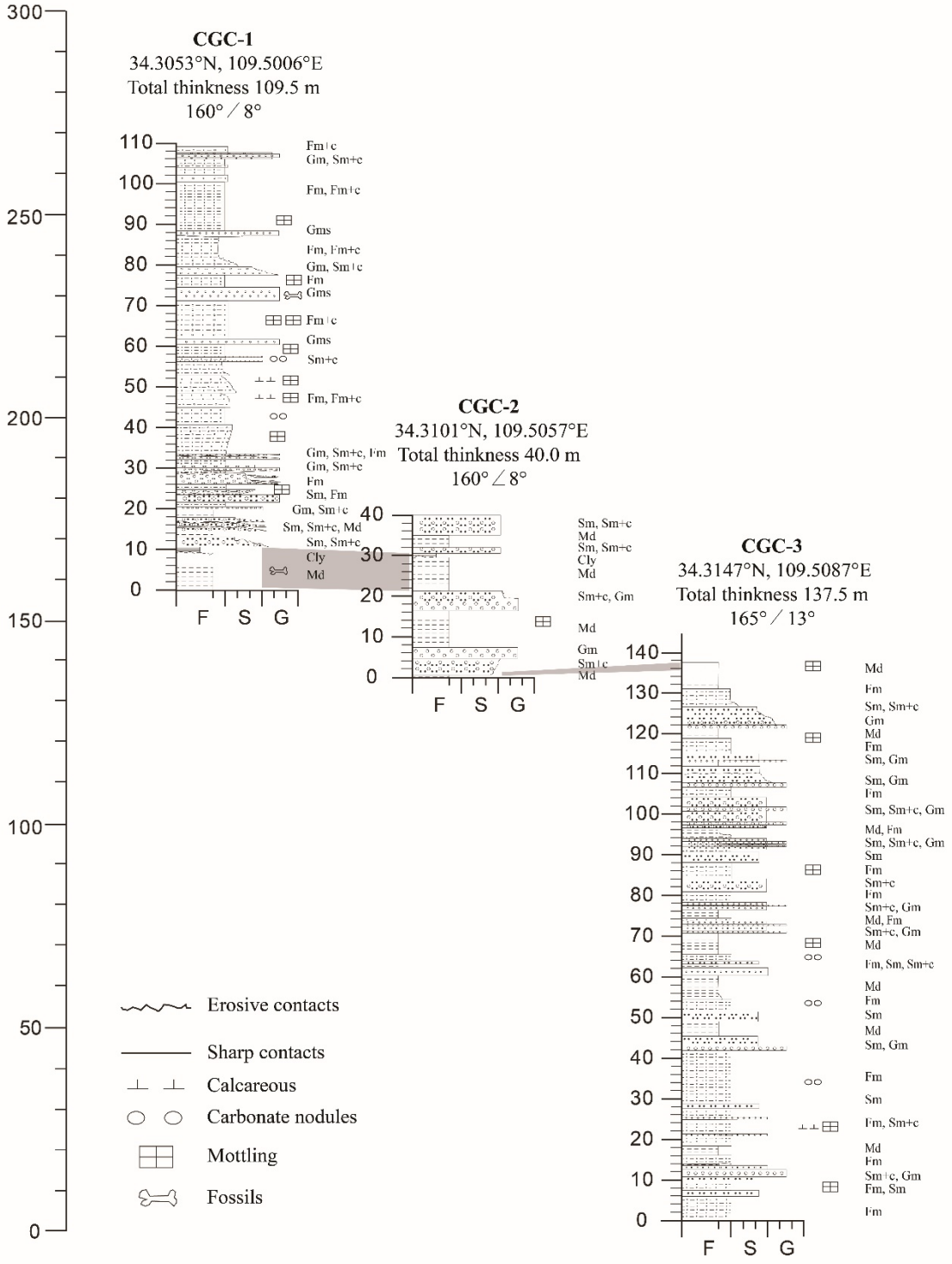
CGC-1
34.3053°N, 109.5006°E
Total thinkness 109.5 m
160° ∕ 8°
CGC-2
34.3101°N, 109.5057°E
Total thinkness 40.0 m
160° ∕ 8°
CGC-3
34.3147°N, 109.5087°E
Total thinkness 137.5 m
165° ∕ 13°
F S G
Erosive contacts
Sharp contacts
Calcareous
Carbonate nodules
Mottling
Fossils

**Fig. S1**

**Section logs and their stratigraphic correlation in the Changgoucun (CGC) sedimentary sequence.** From bottom to top, samples were collected from three subsections at site CGC in the same gully (CGC-3, CGC-2 and CGC-1, respectively).

**Part 2 Interpretation of the high sedimentation rate within chron C3n.2n**

On the basis of the age constraints for each polarity zone, we calculated the sedimentation rate for each zone (Fig. S2). Although average sedimentation rates remain relatively constant, the interval of chron C3n.2n suggests an unusually high sedimentation rate, indicating the deposition of a very thick sedimentary interval in a short period of time. Generally, rapid accumulation rates occur under unique tectonic or climatic influences. If rapid tectonic subsidence occurs, more sediments will be accumulated, and thus the sediments should be coarse-grained. However, the lithology of the C3n.2n interval is mainly thick fine-grained mudstone, with less frequent interbeds of coarse-grained sediments, compared with the other time intervals. This indicates a relatively stable pond-like depositional environment with occasional alluvial inputs. In addition, no sign of fault activity was observed during this interval. Yang et al. (*30*) showed that the climate during this interval (~4.6-4.5 Ma) was the warmest and wettest in the Pliocene. This may have resulted in a stable streamflow that transported sediments to the depocenter. In addition, an alluvial fan tends to migrate continuously. If the alluvial fan migrated to a new location with a relatively large or a concave-shaped space, a favorable accommodation space for rapid sediment accumulation would be provided. Therefore, the unusually high sedimentation rate during chron C3n.2n could be the combined result of alluvial fan migration and long-term climate change. On the other hand, a low transport energy causes both fine-grained sediment accumulation and slow erosion, and therefore a thick sedimentary sequence, such as that corresponding to C3n.2n, was preserved. Erosion did occur in other time intervals and was responsible for the 'missing' 100-kyr cycles in the CGC time series, creating an artifactual 200-kyr 'cycle' in the spectrum.

Another possible reason for the thick fine-grained sediments during the interval corresponding to C3n.2n is lateral facies changes between different outcrops, represented

by a mid-proximal alluvial fan, distal fan, and a lacustrine system (Fig. S3). Because the location of site CGC-2 is closer to the center of the Weihe Basin than site CGC-1, the sedimentary sequence at site CGC-2 consist of rapidly-accumulated thick mudstone. Thus, the different alluvial fan locations have a diversity of sediment accumulation rates, and the interval corresponding to chron C3n.2n, which has a unique position with a high sediment accumulation rate, was thicker than the layers deposited before and afterwards. However, this short interval does not influence the spectral analysis results and the conclusions of this study.

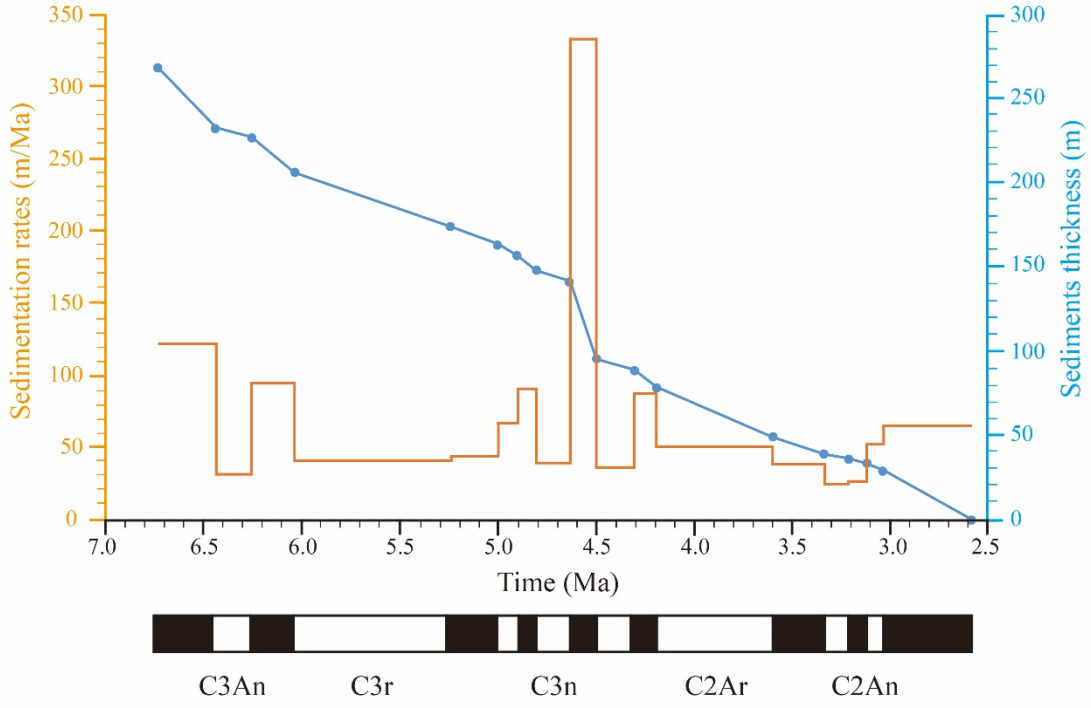


**Fig. S2**

**Sediment accumulation rate in each polarity zone in the Changgoucun (CGC) sedimentary sequence.** Orange line is the sedimentation rate and the blue line is sediment thickness. The polarity column is from chrons C3An to C2An of the Geomagnetic Polarity Time Scale *(21)*; black represents normal polarity and white represents reversed polarity.

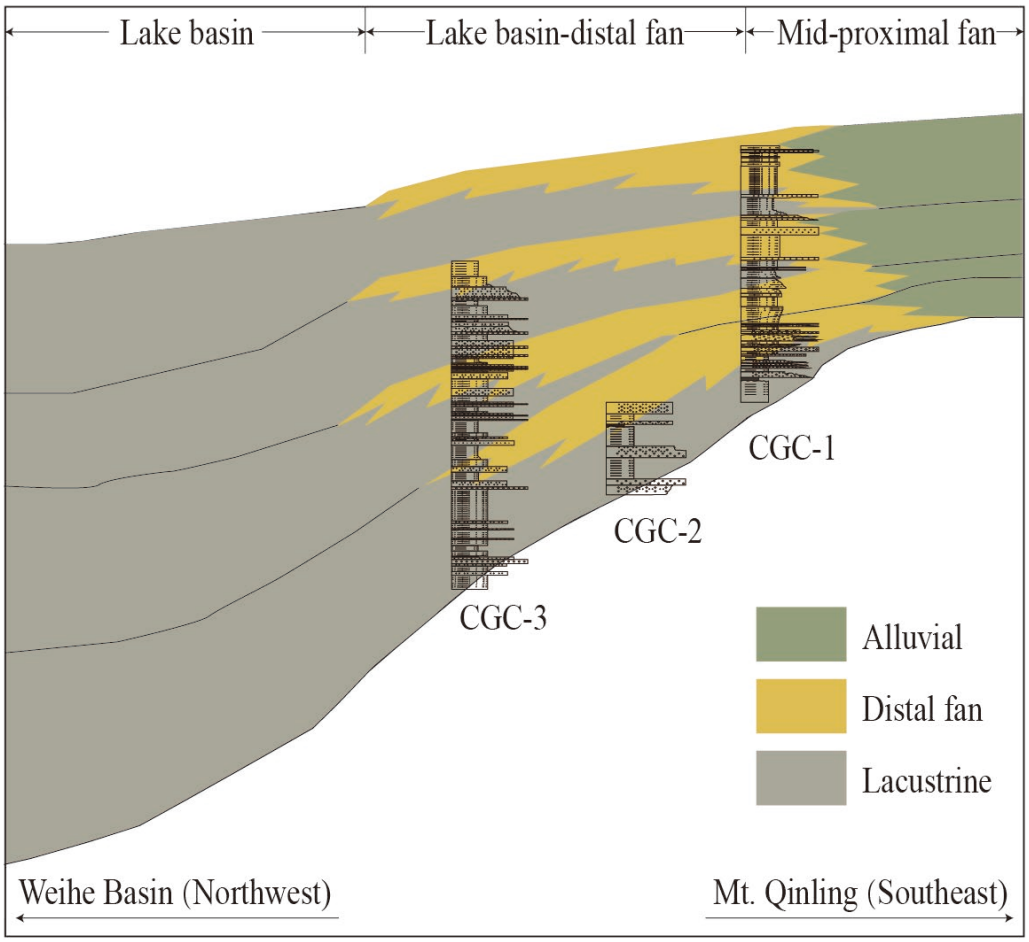


**Fig. S3**

A model of lateral facies changes between different outcrops (modified from *49*) around the Changgoucun (CGC) site.


**Fig. S4**

**The mammalian fossils found during the 2017 field reconnaissance of the Changgoucun (CGC) sedimentary sequence.** This fossil is Bovidae gen. et sp. indet. which was determined by Prof. Zhang Zhaoqun to indicate an age in the Late Miocene, or younger (see the text). (Photo credit: Yichao Wang, School of Geography and Ocean Science, Nanjing University.)

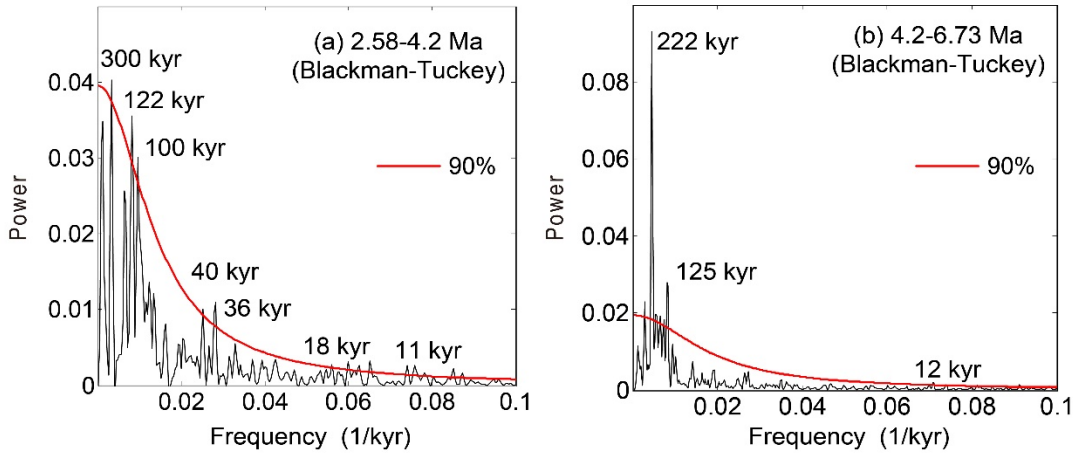


**Fig. S5**

**Blackman-Tukey spectrum analysis results of the mean grain size record for the intervals of (a)** 2.58-4.2 Ma and **(b)** 4.2-6.73 Ma.

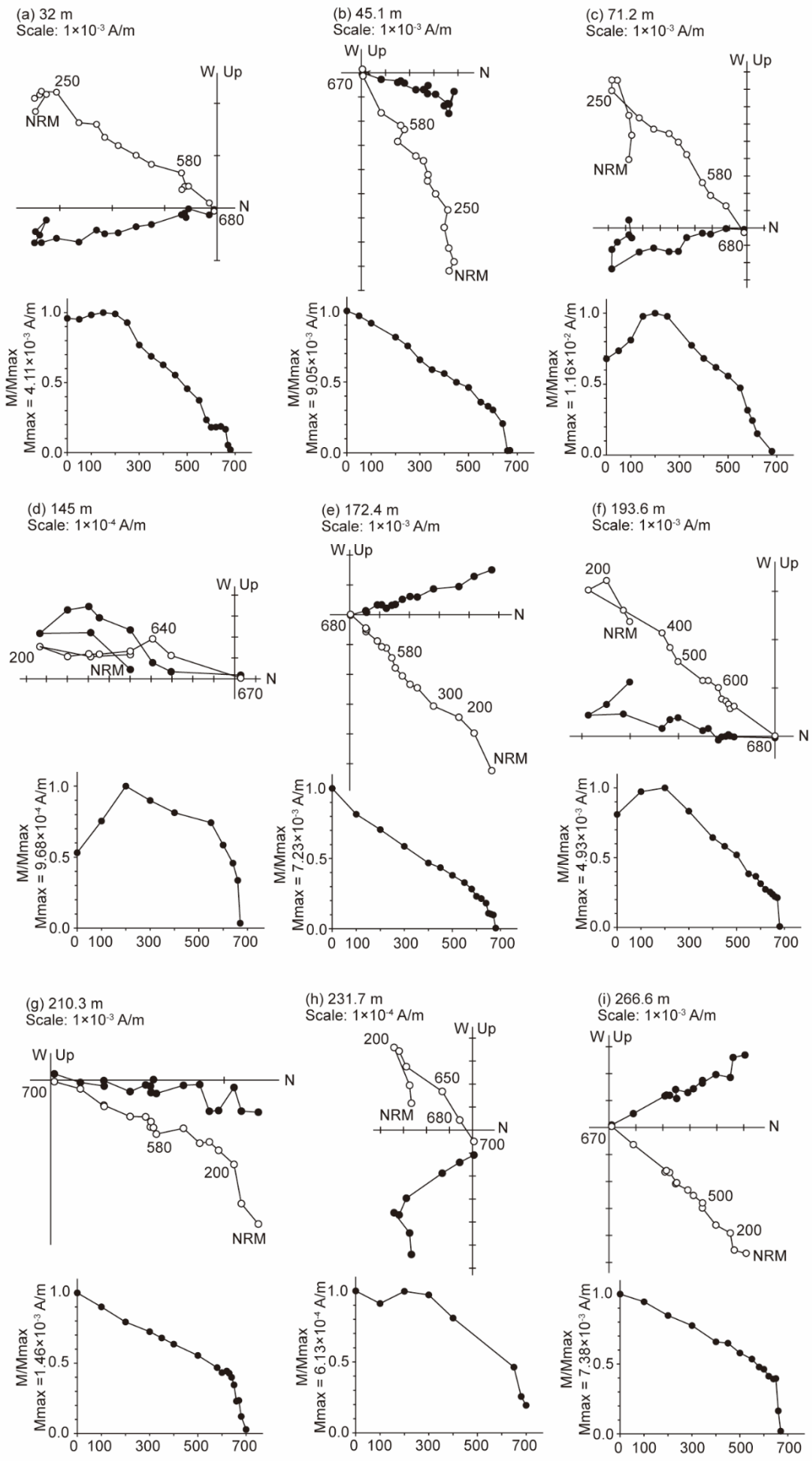
(a) 32 m
Scale: 1×10-3 A/m
W Up
N
250
NRM
580
680
M/Mmax
Mmax = 4.11×10-3 A/m
(b) 45.1 m
Scale: 1×10-3 A/m
W Up
N
670
580
250
NRM
M/Mmax
Mmax = 9.05×10-3 A/m
(c) 71.2 m
Scale: 1×10-3 A/m
W Up
250
NRM
580
N
680
M/Mmax
Mmax = 1.16×10-2 A/m
(d) 145 m
Scale: 1×10-4 A/m
W Up
640
200
NRM
N
670
M/Mmax
Mmax = 9.68×10-4 A/m
(e) 172.4 m
Scale: 1×10-3 A/m
W Up
N
680
580
300
200
NRM
M/Mmax
Mmax = 7.23×10-3 A/m
(f) 193.6 m
Scale: 1×10-3 A/m
W Up
200
NRM
400
500
600
N
680
M/Mmax
Mmax = 4.93×10-3 A/m
(g) 210.3 m
Scale: 1×10-3 A/m
W Up
N
700
580
200
NRM
M/Mmax
Mmax = 1.46×10-3 A/m
(h) 231.7 m
Scale: 1×10-4 A/m
W Up
200
650
NRM
680
N
700
M/Mmax
Mmax = 6.13×10-4 A/m
(i) 266.6 m
Scale: 1×10-3 A/m
W Up
N
670
500
200
NRM
M/Mmax
Mmax = 7.38×10-3 A/m
0.0
0.5
1.0
0 100 300 500 700

**Fig. S6**

**Orthogonal projections and normalized intensity during the progressive thermal demagnetization of representative samples from the Changgoucun (CGC) sedimentary sequence.** Solid (open) circles represent projections onto the horizontal (vertical) plane. Numbers refer to demagnetization temperatures in ℃.

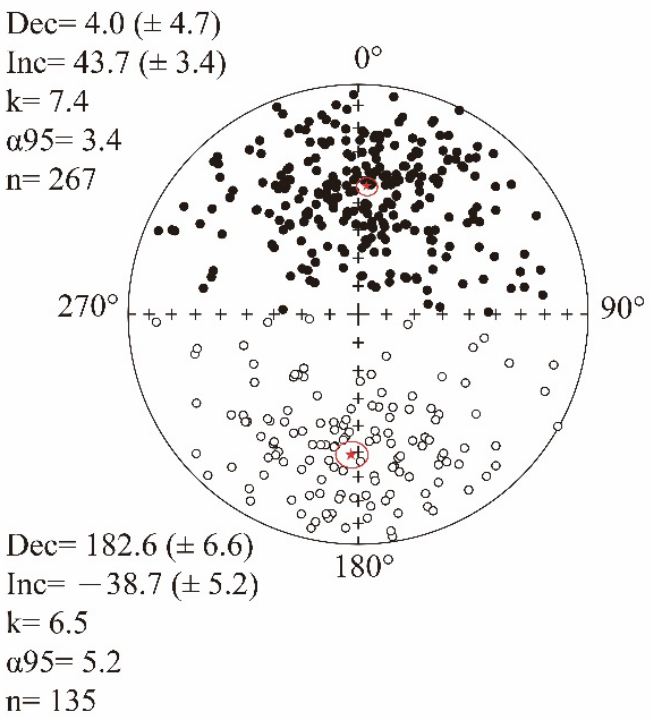


**Fig. S7**

**Stereographic projections of the characteristic remanent magnetization (ChRM) directions.** The solid/open symbols represent projections on the lower/upper hemisphere.

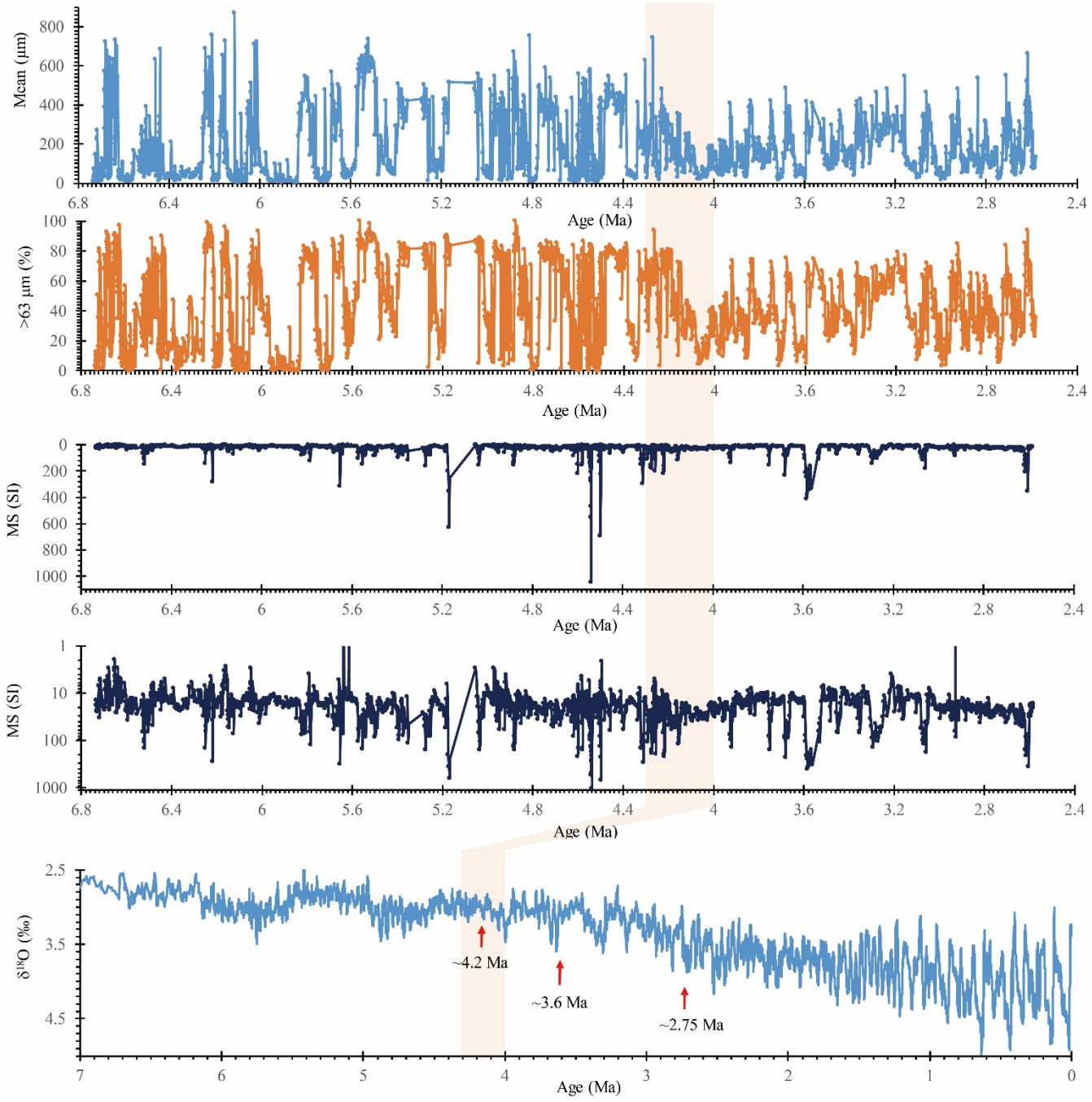
Mean (μm)
800
600
400
200
0
6.8
6.4
6
5.6
5.2
4.8
4.4
4
3.6
3.2
2.8
2.4
Age (Ma)
>63 μm (%)
100
80
60
40
20
0
Age (Ma)
MS (SI)
0
200
400
600
800
1000
Age (Ma)
MS (SI)
1
10
100
1000
Age (Ma)
δ18O (‰)
2.5
3.5
4.5
~4.2 Ma
~3.6 Ma
~2.75 Ma
7
6
5
4
3
2
1
0
Age (Ma)

**Fig. S8**

**Enlarged grain size and magnetic susceptibility time series during 2.58-6.73 Ma for the Changgoucun (CGC) sedimentary sequence in this study, and their comparison with a global ice volume time series since the Late Miocene *(11)*.** There is an obvious high-latitude cooling event at ~4.2 Ma and a high-latitude cooling trend since ~3.6 Ma in the benthic foraminiferal oxygen isotope record. The cooling events at high latitudes in the Northern Hemisphere probably forced the East Asian monsoon precipitation variations on the tectonic time scale.

**Table S1.**

Paleomagnetic data from the Changgoucun (CGC) section.

Depth: stratigraphic level of samples (0 m is the top of the section);

T: temperature steps of the ChRM trajectory;

Dec. and Inc.: declination and inclination of the ChRM direction;

N: number of points/steps used to determine the ChRM direction;

MAD: maximum angular deviation of the best-fit ChRM direction in degrees;

VGP lat: virtual geomagnetic pole latitude derived from the ChRM direction.

| Depth (m) | T (℃) | N | Dec (º) | Inc (º) | MAD (º) | VGP lat. (º) |
|---|---|---|---|---|---|---|
| 0.9 | T450-T670 | 4 | 30.9 | 32.9 | 4.6 | 58 |
| 3.2 | T580-T660 | 4 | 11.9 | 54.1 | 10.7 | 80.2 |
| 3.6 | T550-T670 | 4 | 337.3 | 53.1 | 11 | 71.2 |
| 4 | T500-T680 | 5 | 3.7 | 50 | 3.9 | 85.3 |
| 5.4 | T600-T680 | 6 | 358.6 | 57.8 | 5.7 | 85.7 |
| 6 | T580-T670 | 4 | 318.7 | 41.1 | 12.7 | 52.6 |
| 7 | T450-T680 | 5 | 5.4 | 53.7 | 4.3 | 85.5 |
| 8 | T500-T670 | 5 | 5.8 | 42.7 | 9.5 | 79.2 |
| 9 | T640-T700 | 4 | 34.9 | 22.2 | 6.1 | 50.9 |
| 10 | T500-T680 | 6 | 24.5 | 55.9 | 2.1 | 70 |
| 11 | T580-T680 | 6 | 2.7 | 52.1 | 3 | 87.2 |
| 12 | T550-T670 | 5 | 17 | 33.1 | 8.2 | 67.8 |
| 13.2 | T450-T660 | 4 | 5.9 | 29.9 | 7.7 | 71 |
| 14 | T450-T660 | 7 | 20.8 | 36.8 | 5.6 | 67 |
| 15 | T550-T670 | 5 | 5.6 | 38.3 | 5 | 76.3 |
| 16 | T450-T670 | 7 | 356.1 | 45.8 | 2.4 | 82.2 |
| 17 | T450-T680 | 5 | 6.6 | 32.4 | 4.9 | 72.3 |
| 18 | T500-T680 | 5 | 322.2 | 56.8 | 7.3 | 59.4 |
| 19 | T250-T640 | 5 | 348.1 | 24.3 | 4.7 | 65.9 |
| 21 | T500-T680 | 6 | 50 | 55.5 | 7.8 | 49.5 |
| 22.7 | T500-T680 | 9 | 23.9 | 56.1 | 3.1 | 70.4 |
| 23.4 | T620-T680 | 5 | 13.2 | 39.9 | 8.1 | 73.6 |
| 24.2 | T580-T680 | 7 | 27.4 | 53.6 | 3.8 | 67.4 |
| 24.6 | T400-T670 | 10 | 2.7 | 41.5 | 2.1 | 79.3 |
| 25 | T400-T680 | 7 | 9.1 | 58.5 | 5.6 | 81.2 |
| 26 | T500-T680 | 8 | 354.8 | 43.1 | 5.4 | 79.7 |
| 27.4 | T550-T680 | 6 | 350.6 | 41.8 | 5.4 | 76.9 |
| 27.6 | T550-T670 | 7 | 19.6 | 52.2 | 5.3 | 73.6 |
| 27.8 | T550-T680 | 8 | 359.6 | 39.1 | 2 | 77.8 |
| 28 | T100-T660 | 12 | 347.2 | 49.5 | 4.7 | 78.5 |
| 28.2 | T500-T660 | 7 | 3.6 | 58.4 | 4.2 | 84.4 |
| 28.4 | T450-T660 | 5 | 13.3 | 50.8 | 6.9 | 78.5 |
| 29.2 | T580-T680 | 7 | 203 | 7.3 | 6.7 | -46.3 |
| 29.4 | T600-T670 | 4 | 210 | -7 | 2.3 | -48.5 |
| 31.6 | T500-T680 | 5 | 210.1 | -31.5 | 5 | -58 |
| 32 | T400-T680 | 7 | 166.6 | -32.5 | 3 | -69.5 |
| 32.2 | T640-T680 | 4 | 244.6 | -48.3 | 5.3 | -35.8 |
| 32.4 | T450-T680 | 10 | 154 | -36.5 | 4.5 | -63.1 |
| 32.6 | T500-T660 | 4 | 214.4 | -42.8 | 4.8 | -58.8 |

| | | | | | | |
|---|---|---|---|---|---|---|
| 32.8 | NRM -T580 | 9 | 331 | -28.3 | 5.9 | 33.4 |
| 33 | T600-T680 | 6 | 184.3 | -56.1 | 5.2 | -85.8 |
| 33.2 | T580-T700 | 6 | 199.1 | -48.5 | 11 | -73.1 |
| 33.4 | T450-T680 | 5 | 316.6 | 9.5 | 7 | 40.2 |
| 33.8 | NRM -T500 | 7 | 89 | 42.8 | 11.8 | 14.5 |
| 34 | T600-T680 | 6 | 355.4 | 37.5 | 9.3 | 76.1 |
| 34.2 | T450-T700 | 4 | 292.7 | 6.5 | 6.7 | 20.5 |
| 34.4 | T600-T680 | 3 | 299.8 | 21.9 | 6.2 | 30.9 |
| 34.8 | T200-T620 | 5 | 47.9 | 31.1 | 9.8 | 43.9 |
| 36 | T620-T670 | 4 | 160.1 | -12.1 | 6.1 | -56.3 |
| 37.3 | T550-T670 | 4 | 151.5 | -39 | 9.9 | -62.2 |
| 38.3 | T450-T660 | 5 | 228.7 | -33.9 | 4.2 | -44.1 |
| 38.5 | T450-T670 | 7 | 183.4 | -7.7 | 4.9 | -59.4 |
| 38.7 | T620-T680 | 5 | 212.1 | -27.3 | 8.2 | -54.9 |
| 39.3 | T500-T680 | 5 | 356.2 | 20.3 | 3.9 | 65.9 |
| 39.9 | T580-T670 | 5 | 305.9 | 22.7 | 7 | 36.1 |
| 40.8 | T350-T680 | 7 | 318.3 | 8.9 | 6.6 | 41.2 |
| 41.1 | T400-T680 | 8 | 339 | 16.8 | 5.6 | 57.8 |
| 42.1 | T620-T680 | 4 | 344.1 | 17.7 | 7.7 | 60.8 |
| 43.1 | T600-T680 | 5 | 345.6 | 44.2 | 4.9 | 75 |
| 44.1 | T620-T680 | 3 | 40.1 | 9.5 | 3.8 | 42.6 |
| 44.7 | T640-T670 | 4 | 15.2 | 39.5 | 4.5 | 72.1 |
| 45.1 | T450-T680 | 7 | 16 | 56.5 | 4.2 | 76.7 |
| 45.7 | T450-T660 | 5 | 11.5 | 38 | 5.8 | 73.5 |
| 45.9 | T600-T680 | 4 | 9.1 | 21.2 | 8.2 | 65.2 |
| 46.5 | T300-T660 | 6 | 30.2 | 22.9 | 7.2 | 54.6 |
| 46.9 | T450-T680 | 9 | 16.2 | 39.9 | 5.9 | 71.7 |
| 47.3 | T580 -T670 | 4 | 6.4 | 76.2 | 5.6 | 60.2 |
| 47.6 | T550-T670 | 6 | 156.6 | 33 | 8.6 | -33.2 |
| 49.2 | T200-T580 | 6 | 147.8 | -10.7 | 16 | -48.5 |
| 49.4 | T450-T670 | 4 | 177.4 | -12.3 | 4.3 | -61.8 |
| 49.6 | T450-T660 | 3 | 195 | -19.6 | 8.9 | -62.2 |
| 49.8 | T400-T680 | 5 | 241.2 | -20.9 | 9.2 | -29.8 |
| 50.4 | T620-T670 | 4 | 229.3 | -7.9 | 10.5 | -35.2 |
| 51.2 | T500-T700 | 5 | 151.7 | -51.3 | 6.4 | -66.3 |
| 51.4 | T200-T660 | 10 | 218.5 | -32.7 | 8.8 | -52 |
| 51.6 | T640-T670 | 4 | 206.8 | -28.9 | 7.8 | -59.4 |
| 51.8 | T200-T680 | 8 | 159.5 | -54.5 | 7 | -73.2 |
| 52 | T620-T680 | 5 | 186 | -45.3 | 3.8 | -80.9 |
| 52.4 | T300-T700 | 5 | 150.5 | -37.3 | 13.9 | -60.7 |
| 53.2 | T500-T620 | 3 | 171.2 | -2.4 | 4.6 | -55.9 |
| 53.6 | T300-T670 | 4 | 193.9 | -41.1 | 9.4 | -73.8 |
| 53.8 | T400-T700 | 4 | 185.5 | -32.2 | 4.1 | -72.5 |

| | | | | | | |
|---|---|---|---|---|---|---|
| 54 | T550-T680 | 5 | 196 | -40.7 | 3.8 | -72.2 |
| 55 | T500-T680 | 4 | 206.7 | -57.5 | 7.2 | -68.2 |
| 56 | T450-T700 | 7 | 141.1 | -43.4 | 4.1 | -55.3 |
| 57 | T550-T680 | 4 | 205.5 | -43.1 | 6.1 | -66.1 |
| 58 | T500-T680 | 10 | 189.9 | -41.4 | 3 | -76.4 |
| 59 | T300-T620 | 5 | 167.6 | -68.2 | 6.2 | -70.8 |
| 60 | T500-T680 | 6 | 174.3 | -30.1 | 7 | -71.1 |
| 60.6 | T640-T670 | 4 | 187.5 | -49.8 | 5.2 | -82.7 |
| 61.4 | T550-T680 | 9 | 184.3 | -47.4 | 5 | -83.2 |
| 62 | T350-T680 | 10 | 213.2 | -33.1 | 6.9 | -56.3 |
| 63 | T500-T680 | 4 | 221 | -60.5 | 4.2 | -57.2 |
| 64.1 | T650-T680 | 4 | 225.9 | -57.8 | 9.7 | -53.2 |
| 65 | T400-T670 | 6 | 191.3 | -35.5 | 7 | -72.2 |
| 66 | T400-T680 | 7 | 185.5 | -22.3 | 7.4 | -66.7 |
| 67 | T620-T700 | 3 | 162.5 | -26.8 | 12.4 | -64.4 |
| 68 | T500-T680 | 8 | 191.5 | -47.5 | 3 | -78.7 |
| 69 | T580-T680 | 7 | 186.5 | -52 | 6.8 | -84.3 |
| 70.4 | T450-T680 | 10 | 171.6 | -44.5 | 2.7 | -79.1 |
| 71.2 | T550-T680 | 5 | 171.8 | -47.6 | 4.3 | -81 |
| 72.3 | T500-T660 | 5 | 163.2 | -60.9 | 6.8 | -74.8 |
| 73.3 | T350-T680 | 9 | 146.5 | -54.9 | 6.1 | -62.6 |
| 74.1 | T500-T680 | 4 | 189 | -33.2 | 4.3 | -71.9 |
| 75.1 | T300-T680 | 8 | 192.7 | -50.2 | 5.3 | -78.8 |
| 76.3 | T250-T670 | 6 | 165.8 | -45.8 | 6.2 | -75.9 |
| 77.2 | T400-T680 | 4 | 141.5 | -26.6 | 6.2 | -49.8 |
| 78.1 | T400-T670 | 6 | 200 | -29 | 5.6 | -64 |
| 78.3 | T400-T700 | 5 | 265 | -57.6 | 10.5 | -23.9 |
| 78.6 | T250-T620 | 7 | 167.5 | -56.1 | 6.3 | -79.6 |
| 83 | T600-T680 | 6 | 28.3 | 46.3 | 2.6 | 64.9 |
| 83.4 | T620-T680 | 4 | 353.5 | 54.5 | 8.9 | 84.6 |
| 84 | T600-T680 | 4 | 47.1 | 19.5 | 12.6 | 40.7 |
| 85 | T150-T350 | 4 | 326.2 | 42.6 | 6.5 | 59.2 |
| 85.6 | T550-T680 | 5 | 38.6 | 71.7 | 6.6 | 55.7 |
| 88 | T400-T640 | 6 | 320.7 | 66.1 | 5.6 | 57.8 |
| 88.6 | T100-T670 | 7 | 31.3 | 18.5 | 6.9 | 52.1 |
| 90.2 | T500-T680 | 6 | 186.7 | -44.2 | 3.4 | -79.8 |
| 91 | T550-T700 | 6 | 164.4 | -35.4 | 6.8 | -69.8 |
| 91.2 | T400-T640 | 5 | 159.4 | -17.8 | 9.2 | -58.5 |
| 91.4 | T400-T670 | 5 | 199.3 | -39.8 | 7.3 | -69.5 |
| 92.2 | T550-T700 | 4 | 143.7 | -42.5 | 8.3 | -57.1 |
| 92.6 | T500-T680 | 5 | 174.2 | -28.1 | 4.5 | -69.9 |
| 95.4 | T550-T640 | 5 | 106.1 | -46.8 | 12.9 | -27.8 |
| 95.6 | T450-T700 | 6 | 27.4 | 20.9 | 11.2 | 55.7 |

| | | | | | | |
|---|---|---|---|---|---|---|
| 98.9 | T550-T680 | 6 | 350.7 | 15.3 | 6 | 62.1 |
| 99.1 | T550-T680 | 8 | 301.8 | 11.9 | 2.3 | 29.5 |
| 100.1 | T450-T680 | 7 | 336 | 40.9 | 1.7 | 66.4 |
| 101 | T550-T670 | 7 | 6.8 | 64.7 | 3.8 | 76.7 |
| 101.4 | T500-T660 | 7 | 311.1 | 66.3 | 1.9 | 51.4 |
| 102 | T500-T680 | 8 | 16.5 | 60.6 | 6 | 75.1 |
| 103 | T640-T680 | 4 | 17.2 | 20.9 | 4 | 61.7 |
| 104 | T550-T680 | 8 | 358.1 | 41.1 | 3.2 | 79.1 |
| 105 | T580-T680 | 6 | 356 | 25.2 | 4.4 | 68.6 |
| 106 | T550-T680 | 7 | 16.9 | 48.7 | 5.2 | 74.9 |
| 107.2 | T500-T680 | 9 | 5.2 | 24 | 4.6 | 67.7 |
| 108.1 | T550-T670 | 5 | 24.6 | 15.5 | 4 | 55.2 |
| 109 | T450-T680 | 7 | 31.6 | 40.2 | 4.4 | 60.2 |
| 109.5 | T550-T680 | 5 | 25 | 37.4 | 8 | 64.2 |
| 109.7 | T200-T680 | 5 | 341.9 | 44.4 | 6.8 | 72.4 |
| 111.8 | T200-T580 | 7 | 315.6 | 36.7 | 13.9 | 48.6 |
| 113 | T200-T680 | 7 | 326.6 | 15.3 | 10 | 49.4 |
| 114.6 | T580-T680 | 8 | 320.1 | 45.7 | 3.5 | 55.2 |
| 114.8 | T550-T680 | 9 | 7.2 | 27.7 | 2.1 | 69.3 |
| 115.4 | T550-T680 | 8 | 349.6 | 38.9 | 5.1 | 74.6 |
| 115.7 | T600-T700 | 8 | 324.1 | 29.9 | 2.8 | 53 |
| 116.6 | T300-T580 | 6 | 14.7 | 48.1 | 5.6 | 76.5 |
| 116.8 | T650-T680 | 4 | 15.2 | 56 | 8.1 | 77.4 |
| 117.3 | T660-T700 | 4 | 21.1 | 11.5 | 2 | 55.5 |
| 117.5 | T650-T680 | 4 | 22.2 | 31.4 | 1 | 63.6 |
| 117.7 | T650-T680 | 4 | 35.4 | 17.9 | 2.3 | 49 |
| 117.9 | T650-T680 | 4 | 18.7 | 28.5 | 2.3 | 64.5 |
| 118.1 | T580-T670 | 4 | 342.4 | 72.7 | 5.3 | 63.5 |
| 118.3 | T640-T680 | 4 | 20.5 | 25.8 | 4.7 | 62.2 |
| 118.7 | T580-T670 | 4 | 308.5 | 51.5 | 5.3 | 47.3 |
| 118.9 | T580-T700 | 4 | 6.9 | 24.4 | 4.7 | 67.6 |
| 119.1 | T640-T680 | 4 | 30.3 | 28.5 | 8.3 | 56.7 |
| 119.3 | T450-T580 | 4 | 33.9 | 53.8 | 4.1 | 62.1 |
| 119.5 | T600-T670 | 4 | 21.6 | 34.4 | 8 | 65.4 |
| 119.9 | T450-T670 | 9 | 10.4 | 38.9 | 5.3 | 74.6 |
| 120.1 | T580-T660 | 5 | 309.3 | 64.3 | 7.4 | 50.3 |
| 120.4 | T300-T670 | 7 | 346.9 | 50.8 | 3.9 | 78.7 |
| 120.8 | T500-T670 | 7 | 0.6 | 25.3 | 9.6 | 69 |
| 121 | T500-T680 | 8 | 5 | 50.6 | 6.8 | 84.8 |
| 121.2 | T550-T640 | 4 | 342.3 | 16.4 | 7.4 | 59.4 |
| 121.4 | T400-T670 | 5 | 346.4 | 41.6 | 4.2 | 74.3 |
| 121.6 | T600-T700 | 6 | 347.4 | 41.5 | 5.4 | 74.8 |
| 121.8 | T550-T670 | 5 | 61 | 12.4 | 11.9 | 27.4 |

| | | | | | | |
|---|---|---|---|---|---|---|
| 122 | T550-T680 | 5 | 327.6 | 35.5 | 6.4 | 57.8 |
| 122.2 | T600-T680 | 5 | 59 | 58.9 | 7 | 43.4 |
| 122.4 | T300-T550 | 5 | 5.2 | 41.4 | 5.7 | 78.5 |
| 122.8 | T450-T660 | 6 | 12.7 | 13.1 | 7.3 | 59.9 |
| 123 | T450-T630 | 4 | 44.2 | 52.7 | 4.1 | 53.5 |
| 123.2 | T400-T640 | 6 | 53.4 | 49 | 5.5 | 45.1 |
| 123.4 | T600-T670 | 4 | 16.9 | 57.3 | 5.8 | 75.9 |
| 126.8 | T600-T680 | 6 | 35.7 | 22.4 | 3 | 50.4 |
| 127.2 | T600-T660 | 4 | 357.6 | 52.9 | 3.5 | 87.8 |
| 127.6 | T580-T670 | 6 | 31.4 | 33.8 | 6 | 57.9 |
| 128 | T550-T670 | 5 | 25.5 | 78.6 | 5.8 | 53.3 |
| 128.5 | T300-T660 | 6 | 333.2 | 34.8 | 8.1 | 61.8 |
| 128.7 | T500-T670 | 8 | 1.4 | 30.2 | 3.7 | 71.9 |
| 128.9 | T550-T650 | 5 | 21.3 | 10.4 | 3.5 | 54.9 |
| 129.1 | T550-T700 | 4 | 35.4 | 11.3 | 6.4 | 46.6 |
| 129.3 | T200-T670 | 9 | 327.3 | 33.8 | 7.4 | 56.9 |
| 129.5 | T450-T670 | 5 | 43.1 | 41.7 | 6.9 | 51.3 |
| 129.8 | T600-T670 | 5 | 19.6 | 25.7 | 3.6 | 62.7 |
| 130.3 | T640-T700 | 5 | 3.4 | 41.8 | 3 | 79.4 |
| 130.5 | T200-T650 | 8 | 350.3 | 47.1 | 6.3 | 79.8 |
| 130.7 | T600-T680 | 6 | 5.4 | 38.7 | 2 | 76.6 |
| 131.2 | T580-T650 | 5 | 3.3 | 66.4 | 4.6 | 75.3 |
| 131.4 | T500-T670 | 7 | 5.7 | 63.4 | 3.2 | 78.5 |
| 132 | T630-T680 | 5 | 322.8 | 49 | 6.2 | 58.4 |
| 132.4 | T450-T660 | 6 | 354 | 53 | 5.2 | 85 |
| 133 | T640-T680 | 5 | 30.9 | 32.6 | 4.4 | 57.9 |
| 133.2 | T500-T670 | 8 | 29.5 | 32.4 | 4.8 | 58.8 |
| 134 | T640-T700 | 6 | 357.6 | 31.9 | 2.8 | 72.8 |
| 134.4 | T580-T680 | 7 | 356.2 | 30.7 | 3.4 | 71.9 |
| 134.6 | T600-T680 | 7 | 343.9 | 35.2 | 5.4 | 69.4 |
| 135.2 | T600-T680 | 7 | 349.7 | 13 | 2.6 | 60.7 |
| 136 | T580-T680 | 8 | 347.7 | 67.5 | 4.1 | 71.6 |
| 136.4 | T450-T640 | 6 | 346.2 | 65.9 | 4.7 | 72.7 |
| 137 | T600-T670 | 6 | 3.5 | 50.6 | 7.2 | 85.8 |
| 137.8 | T550-T670 | 4 | 341.9 | 30.8 | 3.9 | 66 |
| 138 | T400 -T700 | 5 | 45.1 | 52.3 | 6.7 | 52.7 |
| 138.4 | T550-T680 | 8 | 332.6 | 49.2 | 1.9 | 66.5 |
| 139 | T580-T680 | 5 | 8.4 | 35.6 | 5.2 | 73.6 |
| 139.4 | T500-T640 | 6 | 316 | 36.8 | 2.3 | 48.9 |
| 140 | T500-T680 | 7 | 334.1 | 48.9 | 3 | 67.7 |
| 140.8 | T620-T680 | 4 | 60.9 | 39.6 | 13.5 | 35.9 |
| 141.2 | T200-T680 | 14 | 178.3 | 50.5 | 7.9 | -24.4 |
| 141.4 | T650-T680 | 4 | 20.1 | 21.2 | 8 | 60.3 |

| | | | | | | |
|---|---|---|---|---|---|---|
| 141.6 | T550-T650 | 5 | 192.4 | -5.4 | 6.3 | -56.4 |
| 142 | T400-T670 | 4 | 156.6 | -39.9 | 10.8 | -66.5 |
| 145 | T580-670 | 5 | 187.5 | -13.6 | 8.1 | -61.7 |
| 146 | T500-T670 | 6 | 171.4 | -5.3 | 8.5 | -57.3 |
| 147.2 | T450-T660 | 8 | 149.7 | -28.8 | 14.9 | -56.8 |
| 148.4 | T500-T670 | 10 | 17.7 | 32.9 | 2.8 | 67.2 |
| 148.6 | T300-T670 | 11 | 9.7 | 62.4 | 2.1 | 78 |
| 148.8 | T640-T680 | 5 | 5.5 | 40 | 2.1 | 77.5 |
| 149 | T550-T670 | 9 | 15.2 | 37 | 4.3 | 70.8 |
| 149.4 | T450-T700 | 7 | 346.1 | 47.5 | 3.2 | 76.9 |
| 149.6 | T450-T680 | 4 | 323.1 | 62.7 | 147 | 60.1 |
| 149.8 | T620-T680 | 3 | 329.9 | 51.4 | 7.9 | 64.8 |
| 150.3 | NRM -T650 | 9 | 24.3 | 65.7 | 10.7 | 67.4 |
| 150.6 | T450 -T700 | 5 | 305 | 69.2 | 7.2 | 47.3 |
| 150.8 | T400-T680 | 7 | 351.2 | 56.2 | 9.2 | 82.4 |
| 151 | T350-T670 | 6 | 9.7 | 58.7 | 2.5 | 80.7 |
| 151.6 | T100-T680 | 6 | 56.9 | 52.3 | 7.6 | 43.2 |
| 152 | T640-T670 | 4 | 339.4 | 7.6 | 9.8 | 54 |
| 152.2 | T500-T640 | 5 | 348.5 | 47 | 7.9 | 78.4 |
| 153 | T580-T680 | 6 | 14.6 | 67.2 | 6.8 | 71.1 |
| 153.4 | T450-T670 | 9 | 335.8 | 63.5 | 8 | 68.6 |
| 153.6 | T400-T680 | 7 | 329.6 | 51.5 | 3.7 | 64.6 |
| 153.8 | NRM -T580 | 9 | 4.4 | 76.5 | 6.9 | 59.8 |
| 155.8 | T550-T680 | 10 | 29.2 | 44.6 | 4.9 | 63.6 |
| 156.4 | T580-T680 | 8 | 20.2 | 26.5 | 3.9 | 62.7 |
| 156.8 | T640-T680 | 5 | 50.5 | 35.3 | 3.8 | 43.1 |
| 158.3 | T550-T670 | 7 | 212 | -11.6 | 2.8 | -49 |
| 159.5 | T450-T680 | 10 | 191.6 | -8.7 | 3.3 | -58.2 |
| 160.5 | T450-T670 | 5 | 198.4 | -33.6 | 4.5 | -67.1 |
| 162.1 | T600-T680 | 8 | 210.4 | -20.1 | 6.4 | -53.3 |
| 162.3 | T550-T680 | 5 | 219.6 | -14.9 | 5.1 | -44.8 |
| 162.7 | T550-T680 | 4 | 188.5 | -11.7 | 7.8 | -60.5 |
| 162.9 | T550-T680 | 4 | 219.6 | -39.6 | 7.1 | -53.5 |
| 163.1 | T300-T700 | 7 | 256.3 | -27.8 | 9.9 | -19.4 |
| 163.3 | T500-T640 | 5 | 264.6 | -72.7 | 5.9 | -31.3 |
| 163.5 | T660-T700 | 4 | 225.9 | -33.3 | 7.3 | -46.2 |
| 163.9 | T640-T670 | 4 | 119.3 | -0.5 | 7.9 | -24 |
| 164.3 | T580-T700 | 5 | 67 | 35.8 | 11 | 29.7 |
| 166.1 | T450-T670 | 9 | 358.3 | 45.3 | 2.1 | 82.4 |
| 172 | T500-T680 | 11 | 26.6 | 40 | 3 | 64 |
| 172.2 | T300-T660 | 4 | 339.1 | 47.5 | 11.7 | 71.3 |
| 172.4 | T400-T680 | 12 | 345.1 | 46.5 | 2.8 | 75.7 |
| 172.6 | T600-T700 | 8 | 5.2 | 29.5 | 2.4 | 70.9 |

| | | | | | | |
|---|---|---|---|---|---|---|
| 172.8 | T650-T680 | 4 | 300.5 | 31.9 | 1.9 | 34.6 |
| 173 | T580-T680 | 9 | 17.9 | 45.1 | 4.5 | 72.8 |
| 173.2 | T550 -T680 | 9 | 139.3 | 34 | 3.6 | -24.4 |
| 173.4 | T640-T700 | 4 | 8.5 | 56.5 | 13.2 | 82.6 |
| 173.6 | T550-T670 | 7 | 28.3 | 53.4 | 11.6 | 66.6 |
| 174 | T600-T680 | 7 | 312.3 | 25.5 | 11.1 | 42.2 |
| 174.3 | T660-T700 | 3 | 224.8 | -59.6 | 9.4 | -54.3 |
| 176 | T500-T680 | 8 | 165.3 | -29.9 | 4.3 | -67.5 |
| 177.3 | T450-T700 | 7 | 148.4 | -29.8 | 6.3 | -56.3 |
| 177.5 | T640-T700 | 5 | 122.6 | -43.9 | 6 | -40.2 |
| 177.9 | T620-T700 | 3 | 146.1 | -72.2 | 12.9 | -57.6 |
| 181.1 | T300-T680 | 12 | 133.7 | -18.3 | 10 | -40.9 |
| 181.7 | T600-T680 | 6 | 154.5 | -20.1 | 11.1 | -56.6 |
| 182.1 | T200-T670 | 12 | 254.8 | -47.2 | 9.6 | -27.3 |
| 182.3 | T580-T670 | 6 | 226.5 | -58.9 | 5.8 | -52.9 |
| 182.9 | T400-T500 | 3 | 225.2 | -62.8 | 4.7 | -54.1 |
| 183.1 | T300-T670 | 3 | 254.9 | -9 | 9.4 | -15 |
| 183.4 | T580-T670 | 4 | 101.3 | -72.1 | 7.1 | -34.1 |
| 183.7 | T640-T680 | 4 | 169.9 | -21.6 | 9.4 | -65.1 |
| 183.9 | T500-T680 | 7 | 163.4 | -35.9 | 8.4 | -69.4 |
| 184.1 | T650-T680 | 4 | 199.7 | -15.3 | 6.4 | -57.9 |
| 184.5 | T630-T670 | 5 | 258 | -29.2 | 6.4 | -18.5 |
| 186.4 | T600-T680 | 4 | 175 | -43.8 | 4.9 | -80.3 |
| 187.7 | T580-T680 | 4 | 178.3 | -66.2 | 9.2 | -75.7 |
| 188.1 | T600-T680 | 4 | 188.3 | -11.5 | 3.2 | -60.5 |
| 188.3 | T550-T600 | 3 | 141.6 | -11.1 | 12.6 | -44.4 |
| 188.7 | T580-T680 | 5 | 181.3 | -21.2 | 5 | -66.6 |
| 189.1 | T600-T700 | 9 | 176.2 | -17.5 | 1.8 | -64.4 |
| 189.3 | T600-T700 | 8 | 171.6 | -19.2 | 2.1 | -64.4 |
| 189.7 | NRM -T700 | 7 | 168.6 | -12.8 | 11.4 | -60.2 |
| 190.1 | T650-T680 | 4 | 151.9 | -26.8 | 2.9 | -57.6 |
| 192.4 | T580-T680 | 9 | 231.6 | -30.3 | 5.7 | -40.6 |
| 193 | T500-T680 | 11 | 226.4 | -32.8 | 8.5 | -45.6 |
| 193.6 | T600-T680 | 7 | 179.1 | -36.2 | 3.4 | -75.8 |
| 194 | T580-T680 | 9 | 210.3 | -29.8 | 3.5 | -57.2 |
| 194.5 | T580-T700 | 6 | 177.5 | -22.3 | 2.9 | -67.2 |
| 195.1 | T640-T680 | 5 | 189.1 | -13.1 | 3.5 | -61.1 |
| 195.5 | T580-T680 | 7 | 195.9 | -10.6 | 4.1 | -57.5 |
| 195.8 | T580-T700 | 4 | 192.5 | -27.3 | 3.6 | -67.2 |
| 198.3 | T500-T670 | 10 | 220.9 | -39.7 | 6.1 | -52.4 |
| 198.9 | T500-T680 | 9 | 213.4 | -34 | 3.3 | -56.5 |
| 199.3 | T400-T680 | 13 | 216.3 | -47 | 5.4 | -58.5 |
| 199.7 | T500-T670 | 6 | 208.5 | -40.9 | 4.7 | -62.9 |

| | | | | | | |
|---|---|---|---|---|---|---|
| 200.3 | T500-T680 | 11 | 190.3 | -41 | 2.2 | -75.9 |
| 200.9 | T500-T670 | 8 | 146.1 | -22.5 | 3.5 | -51.8 |
| 201.3 | T550-T680 | 8 | 165.7 | -41.7 | 3.9 | -73.8 |
| 201.9 | T550-T670 | 5 | 167.3 | -32.3 | 5.2 | -69.8 |
| 202.3 | T600-T680 | 7 | 149 | -26.1 | 8.7 | -55.3 |
| 203.3 | T400-T680 | 7 | 126.6 | -52.5 | 8.8 | -46.1 |
| 203.5 | T300-T500 | 4 | 223 | -4.7 | 13.1 | -38.8 |
| 203.9 | T500-T670 | 3 | 107.9 | -31.5 | 2.5 | -24.1 |
| 204.3 | T350-T700 | 5 | 192 | -21.4 | 6.7 | -64.3 |
| 204.5 | T200-T680 | 7 | 159.1 | -9.4 | 5.7 | -54.6 |
| 204.9 | T580-T680 | 4 | 142.2 | -47 | 7.3 | -57.3 |
| 205.1 | T450-T680 | 6 | 137.7 | -12 | 5.2 | -41.8 |
| 205.3 | T500-T700 | 4 | 185.9 | -20.5 | 6.2 | -65.7 |
| 206.1 | T400-T580 | 4 | 163 | -51.3 | 5.6 | -75.6 |
| 206.3 | NRM -T680 | 15 | 186.6 | 53.1 | 6.8 | -21.7 |
| 206.5 | T580-T670 | 6 | 48.4 | 33.7 | 7.3 | 44.3 |
| 208.3 | T200-T660 | 5 | 19.9 | 61.6 | 5.2 | 72.4 |
| 208.5 | T650-T680 | 4 | 353.1 | 17.6 | 2 | 63.9 |
| 208.7 | T580-T660 | 4 | 74.3 | 42.8 | 7.9 | 26.1 |
| 209.1 | T650-T680 | 4 | 30.2 | 23.6 | 1.3 | 54.9 |
| 209.3 | T600-T680 | 8 | 32.1 | 21.4 | 4 | 52.7 |
| 209.9 | T620-T680 | 5 | 40.8 | 50.6 | 6.4 | 55.8 |
| 210.3 | T630-T700 | 7 | 5.4 | 22.9 | 3.6 | 67.1 |
| 211 | T500-T680 | 11 | 53.3 | 68.6 | 4.7 | 48.4 |
| 211.4 | T500-T620 | 4 | 33.2 | 78.6 | 3.9 | 51.4 |
| 211.8 | T600-T640 | 4 | 44.1 | 74.1 | 8.5 | 51.6 |
| 212.4 | T350-T630 | 4 | 57.7 | 65.6 | 9.9 | 45.6 |
| 212.6 | T500-T660 | 5 | 42.4 | 48.9 | 6.7 | 54 |
| 213.3 | T200-T680 | 11 | 358.8 | 4.9 | 8.4 | 58.1 |
| 213.5 | T580-T660 | 4 | 333.2 | 50 | 5.9 | 67.2 |
| 214.3 | T550-T680 | 5 | 17 | 38.8 | 6.3 | 70.6 |
| 215.1 | T580-T680 | 6 | 345.7 | 14.5 | 2.8 | 60 |
| 215.5 | T550-T670 | 6 | 2 | 22.2 | 5.3 | 67.1 |
| 215.9 | T620-T700 | 5 | 342 | 43.6 | 3.5 | 72.1 |
| 216.1 | T650-T680 | 4 | 332.8 | 43 | 9.8 | 64.7 |
| 217.1 | T100-T600 | 5 | 330.6 | 36.4 | 6.5 | 60.5 |
| 217.3 | T650-T680 | 4 | 334.9 | 30.2 | 11.7 | 61.1 |
| 219.8 | T550-T670 | 4 | 333.9 | 30.6 | 10 | 60.6 |
| 220.4 | T580-T700 | 5 | 9.3 | 4.6 | 2 | 56.8 |
| 221 | T300-T670 | 5 | 344.8 | 30.2 | 4.1 | 67.3 |
| 221.3 | T580-T680 | 4 | 52.9 | 25.9 | 7.7 | 38.1 |
| 221.5 | T300-T680 | 10 | 4.4 | 38 | 7.8 | 76.5 |
| 222.3 | T350-T640 | 5 | 349 | 25.8 | 6.8 | 67 |

| | | | | | | |
|---|---|---|---|---|---|---|
| 222.9 | T350-T640 | 9 | 348.5 | 42.1 | 8.8 | 75.9 |
| 224.7 | T400-T670 | 10 | 7.1 | 37.4 | 6.9 | 75.2 |
| 225.9 | T400-T670 | 7 | 26.8 | 13.9 | 10.7 | 53.2 |
| 226.9 | T600-T700 | 4 | 318.5 | 49.4 | 7.5 | 54.9 |
| 227.1 | T670-T700 | 4 | 236.7 | -45.2 | 13.4 | -41.2 |
| 227.3 | T630-T680 | 6 | 100.6 | -43.5 | 7 | -22.3 |
| 227.7 | T640-T670 | 4 | 171.2 | -57 | 14.3 | -82.2 |
| 228.9 | T650-T680 | 4 | 267.8 | -13.2 | 11.8 | -5.6 |
| 230.5 | T200-T680 | 14 | 76.5 | -68.8 | 8.3 | -19.1 |
| 230.7 | T300-T670 | 11 | 36.8 | -67.2 | 6.8 | -0.3 |
| 230.9 | T550-T680 | 7 | 77.6 | -41.8 | 9.1 | -3.9 |
| 231.5 | T200-T700 | 13 | 72.2 | -13.9 | 5.4 | 10.4 |
| 231.7 | T300-T700 | 6 | 130.2 | -33.3 | 8.9 | -43 |
| 232.1 | T500-T700 | 4 | 104.5 | -13.2 | 10.9 | -15.7 |
| 232.3 | T630-T680 | 4 | 112.4 | -13.2 | 10.5 | -22.2 |
| 232.5 | T100-T670 | 5 | 20.7 | 35.6 | 3.7 | 66.6 |
| 232.9 | T550-T670 | 5 | 11.3 | 38.8 | 9.1 | 74.1 |
| 233.5 | NRM -T450 | 4 | 80.4 | 33 | 12.8 | 17.8 |
| 233.9 | T100-T700 | 4 | 338.6 | 14.1 | 9.7 | 56.4 |
| 234.1 | T550-T620 | 4 | 338.6 | 3.5 | 7.1 | 51.8 |
| 234.7 | T620-T700 | 7 | 350.1 | 43.3 | 3 | 77.5 |
| 235.1 | NRM -T300 | 4 | 337.6 | 55.6 | 11.4 | 71.7 |
| 235.3 | T580-T680 | 5 | 70.7 | 64 | 10 | 36.5 |
| 235.7 | T640-T680 | 4 | 328.9 | 19.5 | 1.7 | 52.6 |
| 236.3 | T580-T670 | 4 | 286.8 | 34.6 | 9.2 | 24.2 |
| 236.7 | T640-T700 | 5 | 331 | 31.5 | 2.5 | 58.9 |
| 237.3 | T350-T580 | 4 | 306.1 | 71 | 4.2 | 47.8 |
| 237.5 | T620-T680 | 4 | 309 | 50.1 | 9.5 | 47.3 |
| 237.9 | T400-T680 | 12 | 322.6 | 49.7 | 8.5 | 58.4 |
| 238.3 | T620-T700 | 6 | 350.8 | 24.7 | 3.7 | 67.1 |
| 238.7 | T450-T680 | 4 | 314.8 | 16.5 | 6.8 | 41.2 |
| 239.1 | T450-T670 | 4 | 52.7 | 34 | 9.5 | 40.9 |
| 239.3 | T580-T670 | 4 | 294.5 | 13.5 | 5.5 | 24 |
| 239.7 | T300-T680 | 10 | 330.5 | 14.2 | 5.8 | 51.6 |
| 241 | T550-T620 | 4 | 279.6 | 32.3 | 11.3 | 17.5 |
| 241.2 | T450-T700 | 7 | 273.7 | 63.2 | 6.7 | 25.7 |
| 241.4 | T300-T680 | 15 | 314.7 | 24.4 | 8.3 | 43.7 |
| 241.8 | T600-T680 | 7 | 317.1 | 11.7 | 7.9 | 41.3 |
| 242.4 | T580-T700 | 9 | 330.1 | 34.9 | 6.1 | 59.5 |
| 242.7 | T640-T670 | 4 | 354 | 9.3 | 11.3 | 59.9 |
| 246.9 | T400-T680 | 4 | 294.4 | 12.1 | 8.1 | 23.5 |
| 247.2 | T300-T650 | 6 | 39.9 | 50.8 | 6.8 | 56.6 |
| 247.5 | T400-T680 | 5 | 59.2 | 65.7 | 3.4 | 44.6 |

| | | | | | | |
|---|---|---|---|---|---|---|
| 247.7 | T100-T680 | 5 | 84.9 | 60.7 | 3.3 | 25.5 |
| 248.1 | T620-T680 | 6 | 81.6 | 64.9 | 5.5 | 29.6 |
| 248.3 | T600-T700 | 9 | 84 | 20.4 | 3.9 | 10.8 |
| 248.7 | T200-T680 | 14 | 73.8 | 50.8 | 8.4 | 29.4 |
| 249.1 | T450-T680 | 5 | 49.7 | 13.7 | 5.1 | 36.8 |
| 249.3 | T300-T680 | 13 | 76.3 | 19.5 | 2.6 | 16.9 |
| 249.5 | T300-T700 | 14 | 40.2 | 22.3 | 3.1 | 47 |
| 249.9 | T600-T680 | 7 | 36.9 | 15.8 | 5.7 | 47.1 |
| 250.3 | T600-T700 | 9 | 26.4 | 1.1 | 3.6 | 48.2 |
| 250.9 | T300-T680 | 13 | 29.1 | 33 | 2.9 | 59.4 |
| 251.3 | T580-T680 | 9 | 50.1 | 38 | 2.7 | 44.3 |
| 251.9 | T300-T680 | 13 | 80.7 | 27.6 | 5.1 | 15.8 |
| 252.3 | T600-T680 | 8 | 70.1 | 24.1 | 3.6 | 23.4 |
| 252.8 | T400-T700 | 14 | 17.7 | 44.6 | 3.4 | 72.8 |
| 253.6 | T640-T700 | 6 | 12.2 | 25.7 | 4 | 66.5 |
| 254.2 | T620-T680 | 6 | 24.8 | 34.4 | 3 | 63.1 |
| 255 | T650-T680 | 4 | 75.3 | 27.9 | 2 | 20.3 |
| 256.6 | T400-T680 | 5 | 299.5 | 62.4 | 12.3 | 43.1 |
| 256.9 | T640-T700 | 4 | 14.2 | 41.4 | 3.5 | 73.8 |
| 259 | T400-T680 | 7 | 3 | 35.5 | 4.8 | 75.1 |
| 259.2 | T200-T700 | 9 | 356.9 | 11.7 | 6.1 | 61.5 |
| 259.6 | T620-T700 | 7 | 344.4 | 23.3 | 7.7 | 63.7 |
| 260.6 | T620-T680 | 6 | 6.8 | 22.7 | 2.5 | 66.7 |
| 261.2 | T550-T700 | 10 | 1.3 | 21.3 | 3.1 | 66.7 |
| 262.7 | T620-T680 | 6 | 359.2 | 37.5 | 6.5 | 76.7 |
| 263.6 | T600-T680 | 7 | 12 | 15.6 | 1.9 | 61.4 |
| 264.7 | T600-T670 | 6 | 11.9 | 42 | 5.2 | 75.6 |
| 265.6 | T580-T680 | 8 | 329.8 | 36.8 | 5.4 | 60 |
| 266.6 | T600-T670 | 6 | 332.7 | 34.4 | 3 | 61.3 |
| 267.6 | T450-T670 | 10 | 284.3 | 34.5 | 4 | 22.1 |
| 268.2 | T300-T700 | 14 | 51.1 | 68.8 | 4.3 | 49.8 |

**Data S1. (separate excel format file)**

Raw data comprising the age of each sampling level, the mean grain size (μm), the >63-μm fraction (%), and the magnetic susceptibility ($10^{-8}m^3/kg$) (see the separate Excel file).

**REFERENCES AND NOTES**


1. H. Cheng, R. L. Edwards, A. Sinha, C. Spötl, L. Yi, S. Chen, M. Kelly, G. Kathayat, X. Wang, X. Li, X. Kong, Y. Wang, Y. Ning, H. Zhang, The Asian monsoon over the past 640,000 years and ice age terminations. *Nature* **534**, 640–646 (2016).

2. S. C. Clemens, A. Holbourn, Y. Kubota, K. E. Lee, Z. Liu, G. Chen, A. Nelson, B. Fox-Kemper, Precession-band variance missing from east Asian monsoon runoff. *Nat. Commun.* **9**, 3364 (2018).

3. K. D. Burke, J. W. Williams, M. A. Chandler, A. M. Haywood, D. J. Lunt, B. L. Otto-Bliesner, Pliocene and Eocene provide best analogs for near-future climates. *Proc. Natl. Acad. Sci. U.S.A.* **115**, 13288–13293 (2018).

4. C. M. Brierley, A. V. Fedorov, Z. Liu, T. D. Herbert, K. T. Lawrence, J. P. LaRiviere, Greatly expanded tropical warm pool and weakened hadley circulation in the early Pliocene. *Science* **323**, 1714–1718 (2009).

5. A. C. Ravelo, D. H. Andreasen, M. Lyle, A. O. Lyle, M. W. Wara, Regional climate shifts caused by gradual global cooling in the Pliocene epoch. *Nature* **429**, 263–267 (2004).

6. S. De Schepper, P. L. Gibbard, U. Salzmann, J. Ehlers, A global synthesis of the marine and terrestrial evidence for glaciation during the Pliocene Epoch. *Earth Sci. Rev.* **135**, 83–102 (2014).

7. M. Mudelsee, M. E. Raymo, Slow dynamics of the Northern Hemisphere glaciation. *Paleoceanography* **20**, PA4022 (2005).

8. G. H. Haug, A. Ganopolski, D. M. Sigman, A. Rosell-Mele, G. E. A. Swann, R. Tiedemann, S. L. Jaccard, J. Bollmann, M. A. Maslin, M. J. Leng, G. Eglinton, North Pacific seasonality and the glaciation of North America 2.7 million years ago. *Nature* **433**, 821–825 (2005).

9. T. D. Herbert, K. T. Lawrence, A. Tzanova, L. C. Peterson, R. Caballero-Gill, C. S. Kelly, Late Miocene global cooling and the rise of modern ecosystems. *Nat. Geosci.* **9**, 843–847 (2016).

10. C. Karas, N. Khelif, A. Bahr, B. D. A. Naafs, D. Nürnberg, J. O. Herrle, Did North Atlantic cooling and freshening from 3.65–3.5 Ma precondition Northern Hemisphere ice sheet growth? *Global Planet. Change* **185**, 103085 (2020).

11. J. C. Zachos, G. R. Dickens, R. E. Zeebe, An early Cenozoic perspective on greenhouse warming and carbon-cycle dynamics. *Nature* **451**, 279–283 (2008).

12. L. E. Lisiecki, M. E. Raymo, A Pliocene-Pleistocene stack of 57 globally distributed benthic $\delta^{18}O$ records. *Paleoceanography* **20**, PA1003 (2005).

13. Institute of Vertebrate Paleontology and Paleoanthropology, *Symposium of the Field Conference of Cenozoic of Lantian, Shaanxi* (Chinese Academy of Sciences, 1966)

14. A. Kaakinen, J. P. Lunkka, Sedimentation of the Late Miocene Bahe Formation and its implications for stable environments adjacent to Qinling Mountains in Shaanxi, China. *J. Asian Earth Sci.* **22**, 67–78 (2003).

15. A. Kaakinen, A long terrestrial sequence in Lantian– a window into the late Neogene palaeoenvironments of northern China, thesis, University of Helsinki, Publications of the Department of Geology (2005), pp. 49.

16. H. Lu, H. Z. Zhang, Y. Wang, L. Zhao, H. Wang, W. Sun, H. Y. Zhang, Cenozoic depositional sequence in the Weihe Basin (Central China): A long-term record of Asian monsoon precipitation from the greenhouse to icehouse earth. *Quat. Sci.* **38**, 1057–1067 (2018).

17. Y. Zhang, W. Huang, Y. Tang, H. Ji, Y. You, Y. Tong, S. Ding, X. Huang, J. Zheng, Ed., *Cenozoic Stratigraphy of the Lantian Region, Shaanxi Province* (Science Press, 1978).

18. Z. L. Ding, S. F. Xiong, J. M. Sun, S. L. Yang, Z. Y. Gu, T. S. Liu, Pedostratigraphy and paleomagnetism of a ~7.0 Ma eolian loess–red clay sequence at Lingtai, Loess Plateau, north-central China and the implications for paleomonsoon evolution. *Palaeogeogr. Palaeoclimatol. Palaeoecol.* **152**, 49–66 (1999).

19. Z. An, D. Sun, M. Chen, Y. Sun, L. Li, B. Chen, Red clay sequences in Chinese loess plateau and recorded paleoclimate events of the late Tertiary. *Quat. Sci.* **20**, 435–446 (2000).

20. H. Lu, X. Wang, L. Li, Aeolian sediment evidence that global cooling has driven late Cenozoic stepwise aridification in central Asia. *Geol. Soc. London Spec. Publ.* **342**, 29–44 (2010).

21. J. G. Ogg, Geomagnetic polarity time scale, in *The Geologic Time Scale* (Cambridge Univ. Press, ed. 1, 2012), pp. 85–113.

22. B. Wang, Cenozoic Sedimentary Evolution of the Weihe Basin: Basin-Orogen Coupling and Eolian Sediments, thesis, Nanjing University (2014), pp. 109.

23. J. Laskar, P. Robutel, F. Joutel, M. Gastineau, A. C. M. Correia, B. Levrar, A long-term numerical solution for the insolation quantities of the Earth. *Astron. Astrophys.* **428**, 261–285 (2004).

24. Z. T. Guo, W. F. Ruddiman, Q. Z. Hao, H. B. Wu, Y. S. Qiao, R. X. Zhu, S. Z. Peng, J. J. Wei, B. Y. Yuan, T. S. Liu, Onset of Asian desertification by 22 Myr ago inferred from loess deposits in China. *Nature* **416**, 159–163 (2002).

25. A. Licht, M. van Cappelle, H. A. Abels, J.-B. Ladant, J. Trabucho-Alexandre, C. France-Lanord, Y. Donnadieu, J. Vandenberghe, T. Rigaudier, C. Lécuyer, D. Terry Jr., R. Adriaens, A. Boura, Z. Guo, A. N. Soe, J. Quade, G. Dupont-Nivet, J.-J. Jaeger, Asian monsoons in a late Eocene greenhouse world. *Nature* **513**, 501–506 (2014).

26. H. Wang, H. Lu, L. Zhao, H. Zhang, F. Lei, Y. Wang, Asian monsoon rainfall variation during the Pliocene forced by global temperature change. *Nat. Commun.* **10**, 5272 (2019).

27. Z. Ding, S. Yang, J. Sun, T. Liu, Iron geochemistry of loess and red clay deposits in the Chinese Loess Plateau and implications for long-term Asian monsoon evolution in the last 7.0 Ma. *Earth Planet Sci. Lett.* **185**, 99–109 (2001).

28. S. Yang, Z. Ding, S. Feng, W. Jiang, X. Huang, L. Guo, A strengthened East Asian Summer Monsoon during Pliocene warmth: Evidence from 'red clay' sediments at Pianguan, northern China. *J. Asian Earth Sci.* **155**, 124–133 (2018).

29. G. H. Haug, R. Tiedemann, Effect of the formation of the Isthmus of Panama on Atlantic Ocean thermohaline circulation. *Nature* **393**, 673–676 (1998).

30. J. Liu, J. Tian, Z. Liu, T. D. Herbert, A. V. Fedorov, M. Lyle, Eastern equatorial pacific cold tongue evolution since the late Miocene linked to extratropical climate. *Sci. Adv.* **5**, eaau6060 (2019).

31. N. J. Shackleton, The 100,000-year ice-age cycle identified and found to lag temperature, carbon dioxide, and orbital eccentricity. *Science* **289**, 1897–1902 (2000).

32. D. W. Lea, The 100 000-yr cycle in tropical SST, greenhouse forcing, and climate sensitivity. *J. Climate* **17**, 2170–2179 (2004).

33. J. Imbrie, A. Berger, E. A. Boyle, S. C. Clemens, A. Duffy, W. R. Howard, G. Kukla, J. Kutzbach, D. G. Martinson, A. McIntyre, A. C. Mix, B. Molfino, J. J. Morley, L. C. Peterson, N. G. Pisias, W. L. Prell, M. E. Raymo, N. J. Shackleton, J. R. Toggweiler, On the structure and origin of major glaciation cycles 2. The 100,000-year cycle. *Paleoceanography* **8**, 699–735 (1993).

34. J. R. Toggweiler, Origin of the 100,000-year timescale in Antarctic temperatures and atmospheric $CO_2$, *Paleoceanography* **23**, PA2211 (2008).

35. S. C. Clemens, R. Tiedemann, Eccentricity forcing of Pliocene–early Pleistocene climate revealed in a marine oxygen-isotope record. *Nature* **385**, 801–804 (1997).

36. J. C. Zachos, B. P. Flower, H. Paul, Orbitally paced climate oscillations across the Oligocene/Miocene boundary. *Nature* **388**, 567–570 (1997).

37. M. L. Lantink, J. Davies, P. R. D. Mason, U. Schaltegger, F. J. Hilgen, Climate control on banded iron formations linked to orbital eccentricity. *Nat. Geosci.* **12**, 369–374 (2019).

38. S. C. Clemens, W. L. Prell, Y. Sun, Z. Liu, G. Chen, Southern Hemisphere forcing of Pliocene $\delta^{18}O$ and the evolution of Indo-Asian monsoons. *Paleoceanography* **23**, PA4210 (2008).

39. S. Rutherford, S. D'Hondt, Early onset and tropical forcing of 100,000-year Pleistocene glacial cycles. *Nature* **408**, 72–75 (2000).

40. Y. Sun, Z. An, S. C. Clemens, J. Bloemendal, J. Vandenberghe, Seven million years of wind and precipitation variability on the Chinese Loess Plateau. *Earth Planet. Sci. Lett.* **297**, 525–535 (2010).

41. J. D. A. Zijderveld, A. C. demagnetization of rocks: Analysis of results. *Dev. Solid Earth Geophys.* **3**, 254–286 (2013).

42. J. L. Kirschvink, The least-squares line and plane and the analysis of palaeomagnetic data. *Geophys. J. Int.* **3**, 699–718 (1980).

43. J. P. Cogné, PaleoMac: A Macintosh application for treating paleomagnetic data and making plate reconstructions. *Geochem. Geophys. Geosyst.* **4**, 1007 (2003).

44. P. L. McFadden, M. W. McElhinny, Classification of the reversal test in palaeomagnetism. *Geophys. J. Int.* **103**, 725–729 (1990).

45. Ø. Hammer, D. A. T. Harper, P. D. Ryan, PAST: Paleontological statistics software package for education and data analysis. *Palaeontologia Electronica* **4**, 9 (2001).

46. M. Schulz, M. Mudelsee, REDFIT: Estimating red-noise spectra directly from unevenly spaced paleoclimatic time series. *Comput. Geosci. UK* **28**, 421–426 (2002).

47. J. V. Waters, S. J. Jones, H. A. Armstrong, Climatic controls on late Pleistocene alluvial fans, Cyprus. *Geomorphology* **115**, 228–251 (2010).

48. S. P. Todd, Stream-driven, high-density gravelly traction carpets: Possible deposits in the Trabeg conglomerate formation, SW Ireland and some theoretical considerations of their origin. *Sedimentology* **36**, 513–530 (1989).

49. R. A. Buckley, A. G. Plint, O. A. Henderson, J. R. Krawetz, K. M. Vannelli, Ramp sedimentation across a middle Albian, Arctic embayment: Influence of subsidence, eustasy and sediment supply on stratal architecture and facies distribution, Lower Cretaceous, Western Canada Foreland Basin. *Sedimentology* **63**, 699–742 (2016).